



Short and long range 2D ^{15}N – ^{15}N NMR correlations among peptide groups by novel solid state dipolar mixing schemes

Sungsool Wi¹ · Conggang Li² · Karen Pham³ · Woonghee Lee³ · Lucio Frydman^{1,4}

Received: 4 July 2023 / Accepted: 6 November 2023
© The Author(s), under exclusive licence to Springer Nature B.V. 2023

Abstract

A recently developed homonuclear dipolar recoupling scheme, Adiabatic Linearly FREquency Swept reCOupling (AL FRESKO), was applied to record two-dimensional (2D) ^{15}N – ^{15}N correlations on uniformly ^{15}N -labeled GB1 powders. A major feature exploited in these ^{15}N – ^{15}N correlations was AL FRESKO's remarkably low RF power demands, which enabled seconds-long mixing schemes when establishing direct correlations. These ^{15}N – ^{15}N mixing schemes proved efficient regardless of the magic-angle spinning (MAS) rate and, being nearly free from dipolar truncation effects, they enabled the detection of long-range, weak dipolar couplings, even in the presence of strong short-range dipolar couplings. This led to a connectivity information that was significantly better than that obtained with spontaneously proton-driven, ^{15}N spin-diffusion experiments. An indirect approach producing long-range ^{15}N – ^{15}N correlations was also tested, relying on short (ms-long) ^1H – ^1H mixings schemes while applying AL FRESKO chirped pulses along the ^{15}N channel. These indirect mixing schemes produced numerous long-distance N_i – $\text{N}_{i\pm n}$ ($n = 2 - 5$) correlations, that might be useful for characterizing three-dimensional arrangements in proteins. Once again, these AL FRESKO mediated experiments proved more informative than variants based on spin-diffusion-based ^1H – ^1H counterparts.

Keywords ^{15}N – ^{15}N correlations · Protein structure · Dipolar-driven recoupling · Chirped pulses

Introduction

Homonuclear dipolar correlation schemes operating in unison with magic angle spinning (MAS), are widely used in solid-state NMR (SSNMR) spectroscopy for the structural characterization of selectively or uniformly labeled biological samples (Tycko and Dabbagh 1990; Sun et al. 1995; Kiihne et al. 1998; Bennett et al. 1992; Nielsen et al. 1994; Raleigh et al. 1988; Verel et al. 1998; Lee et al. 1995; Levitt 2002; Szeverenyi et al. 1982; Grommek et al. 2006; Meier 1994; Brinkmann and Levitt 2001; Tycko 2008; Takegoshi et al. 2001, 2003; Morcombe et al. 2004; Paëpe et al. 2008; Lewandowski et al. 2009a; Weingarth et al. 2009, 2010; Hu et al. 2011, 2012; Scholz et al. 2008; Hou et al. 2011, 2013; Wi and Frydman 2020). Most common among these schemes are methods that rely on first-order recoupling effects, such as RFDR (Bennett et al. 1992) and DREAM; (Verel et al. 1998) although efficient and requiring short mixing times to achieve their correlations, such methods may suffer from dipolar truncation effects (Bayro et al. 2009). Thus, when applied to uniformly ^{13}C -labeled samples, these methods deliver mostly short-range ^{13}C – ^{13}C dipolar correlations

✉ Sungsool Wi
sungsool@magnet.fsu.edu

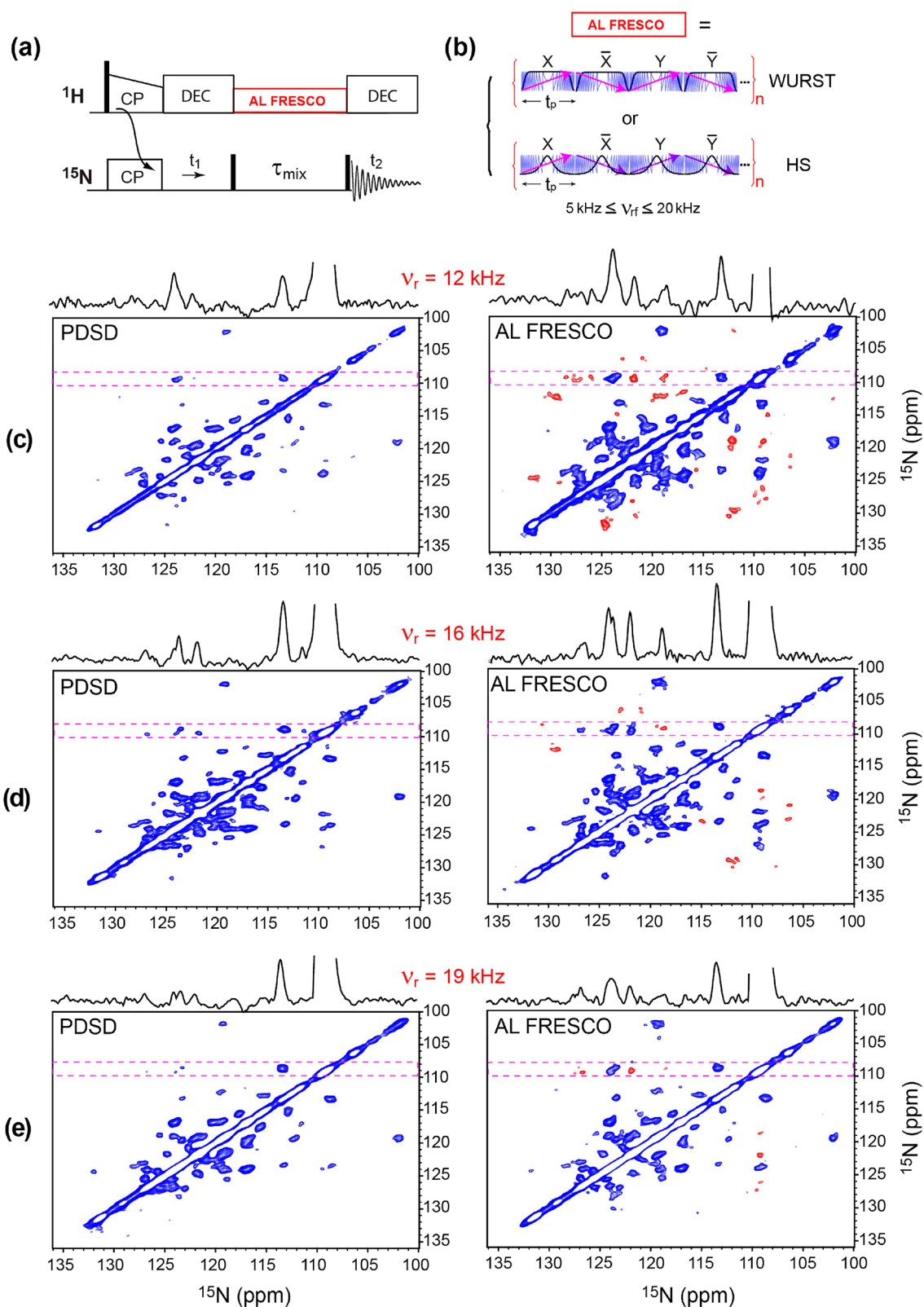
✉ Lucio Frydman
lucio.frydman@weizmann.ac.il

¹ National High Magnetic Field Laboratory, Florida State University, Tallahassee, FL 32304, USA

² Key Laboratory of Magnetic Resonance in Biological Systems, State Key Laboratory of Magnetic Resonance and Atomic and Molecular Physics, National Center for Magnetic Resonance in Wuhan, Wuhan Institute of Physics and Mathematics, Innovation Academy for Precision Measurement Science and Technology, Chinese Academy of Sciences, Wuhan 430071, People's Republic of China

³ Department of Chemistry, University of Colorado at Denver, Denver, CO 80217-3364, USA

⁴ Department of Chemical and Biological Physics, Weizmann Institute of Sciences, Rehovot, Israel



useful for peak assignment purposes, but not for establishing long-range structural constraints. Therefore, although slower in building up dipolar transfers, recoupling schemes

based on second-order effects that are free from dipolar truncation (Takegoshi et al. 2001, 2003; Morcombe et al. 2004), have been utilized in examining weaker, long-range ^{13}C - ^{13}C

Fig. 1 ^{15}N - ^{15}N PDS and AL FRESKO correlation spectra acquired on a doubly-labeled GB1 sample. **a, b** Chirped pulse AL FRESKO sequence implemented within the framework of 2D homonuclear dipolar correlation spectroscopy. A train of four phase-alternating, forward- and backward-swept HS-1 pulses ($t_p = 1.5625$ s) with a relatively weak rf pulse ($5 \text{ kHz} \leq \nu_{rf} \leq 20 \text{ kHz}$) was employed; ^{15}N - ^{15}N PDS correlation spectra would do nothing on the ^1H channel over the mixing period. **c–e** 2D data acquired by spin diffusion (top row) and AL FRESKO schemes (bottom row) at MAS rates of $\nu_r = 12 \text{ kHz}$ (**c**), 16 kHz (**d**), and 19 kHz (**e**). Extra ^{15}N - ^{15}N correlation peaks found in the AL FRESKO scheme but not in PDS, are indicated by red contours. A horizontal projection taken in the $108\text{--}110$ ppm range is shown on top of each 2D spectrum. The number of t_1 increments (n_{t_1}), total number of scans (ns), dwell time of the indirect time domain (dw_{t_1}), and acquisition delay (d_1) used for each spectrum were $n_{t_1} = 160$, ns = 48, $dw_{t_1} = 250 \mu\text{s}$, and $d_1 = 1.2$ s, respectively. Double $^{13}\text{C}/^{15}\text{N}$ labeling was used for facilitating the peaks' assignments (see Supporting Information). Although ^{13}C decoupling was assayed, it did not afford any improvements in the observed line shapes along either dimension and hence its use was discontinued

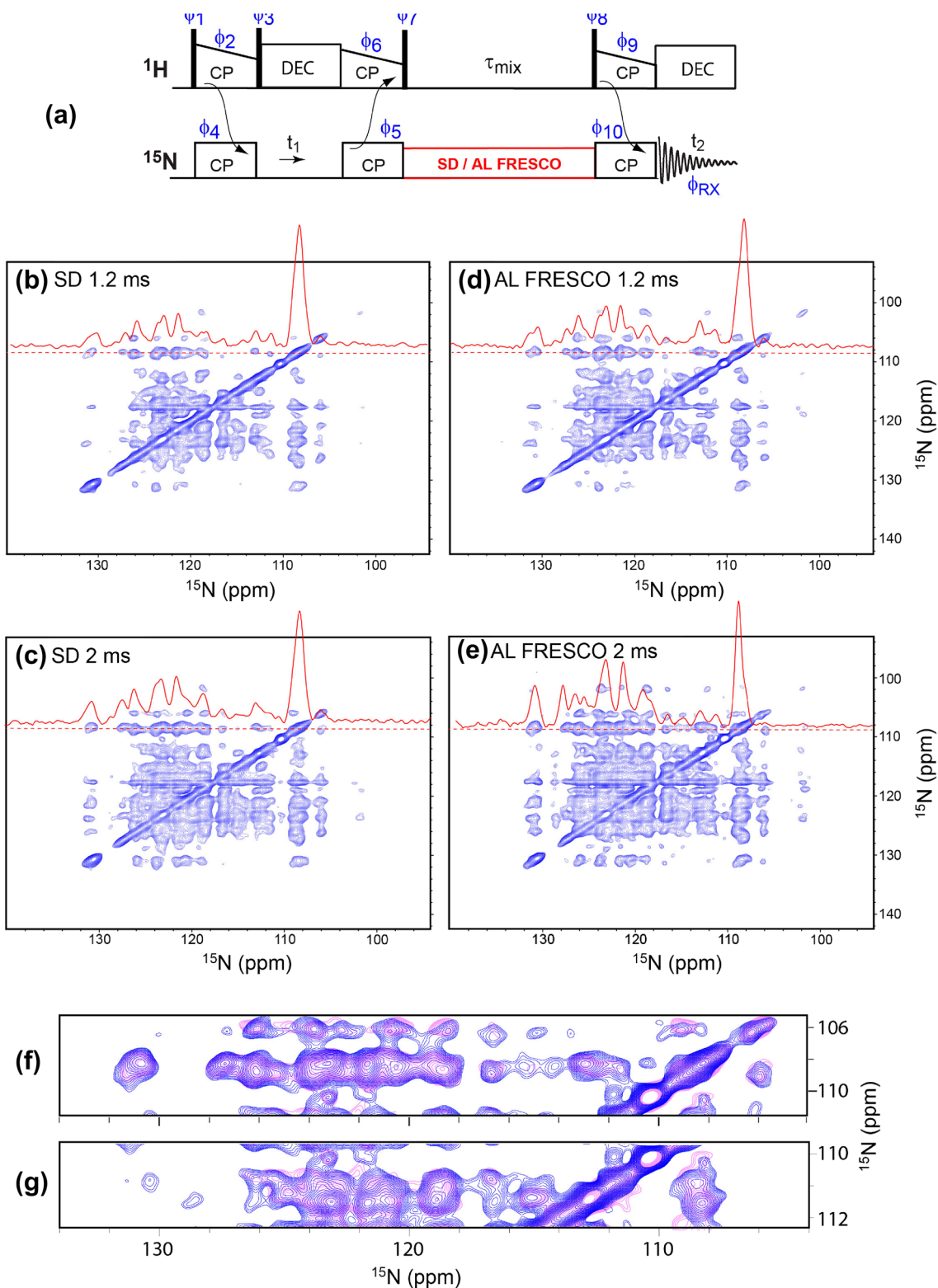
dipolar couplings. Such recoupling schemes include PDS (Szeverenyi et al. 1982; Grommek et al. 2006; Meier 1994), DARR (Takegoshi et al. 2001, 2003), RAD (Morcombe et al. 2004), PARIS_{xy} (Weingarth et al. 2009, 2010), SHANGHAI (Hu et al. 2011), SHA+ (Hu et al. 2012; Shen et al. 2013; Yan and Hu 2016), CORD (Hou et al. 2011, 2013), MIRROR (Scholz et al. 2008), and AL FRESKO (Wi and Frydman 2020). A common feature shared by these recoupling schemes is their utilization of ^1H - ^{13}C heteronuclear dipolar interactions to broaden otherwise narrow ^{13}C - ^{13}C rotational resonance conditions, and thereby facilitate ^{13}C - ^{13}C spin-diffusion despite chemical shifts differences spanning a wide range of frequencies (Takegoshi et al. 2001, 2003). Second-order recoupling methods will usually require longer mixing times than first-order recoupling schemes, and each method will possess its own strengths and weaknesses in terms of the “broadband-ness” of offset frequency differences over which it can recouple, of the MAS rates that it can tolerate, of the radiofrequency (rf) pulse strengths required, etc. (Weingarth et al. 2009, 2010; Hu et al. 2011, 2012; Hou et al. 2011, 2013; Wi and Frydman 2020; Shen et al. 2013). Still, in general, most second-order recoupling schemes have been successfully applied to ^{13}C - ^{13}C dipolar correlation experiments in biomolecules.

Much fewer, by contrast, has been the execution of these experiments to the recoupling of ^{15}N - ^{15}N spin pairs—characterized as they are by weaker dipolar interactions (Reif et al. 2000; Franks et al. 2006; Lewandowski et al. 2009b; Goldbourt et al. 2007; Giraud et al. 2007; Marulanda et al. 2004; Siedel et al. 2005; Donovan et al. 2017; Rossum et al. 2003) and ^{15}N - ^{15}N distance constraints, however, offer a unique potential in the characterization of secondary structures and their three-dimensional arrangements, particularly when dealing with uniformly ^{15}N -labeled proteins. 2D correlations targeting the amide region will then provide one

nitrogen resonance per amino acid residue, thereby facilitating both the assignment and the structural constraint of peptides in the protein. Still, ^{15}N - ^{15}N SSNMR dipolar correlations have usually been reported for $^{15}\text{N}_i$ - $^{15}\text{N}_{i\pm 1}$ connectivities between nearby residues (Franks et al. 2006; Giraud et al. 2007; Marulanda et al. 2004; Siedel et al. 2005; Donovan et al. 2017; Rossum et al. 2003). Major limitations arising when seeking longer correlations in uniformly ^{15}N -labeled proteins include: (1) the aforementioned weakness of the ^{15}N - ^{15}N dipolar interaction, which is only $\approx 1/6$ as strong as a similarly-distanced ^{13}C - ^{13}C dipolar interaction; (2) the relatively long ^{15}N - ^{15}N distances involved when considering non-consecutive—and even consecutive—peptide residues; and (3) the relatively narrow chemical shift dispersion of amide ^{15}N s in proteins (~ 35 ppm), leading to an overlap between ^{15}N peaks that can be severe—particularly when the crystallinity of a protein sample is poor and when seeking multiple correlations. As a result of the first two features, second-order recoupling methods applied to ^{15}N - ^{15}N correlations require significantly longer mixing times than their ^{13}C - ^{13}C counterparts—lasting up to a few seconds. Thus, among all the 2nd-order homonuclear recoupling schemes mentioned above, only the proton-driven spin-diffusion (PDS) scheme that does not require any rf pulses during the mixing, has been so far utilized to achieve these ^{15}N - ^{15}N correlations. The relative inefficiency of PDS, however, also means that the NMR signals will decay significantly by T_1 relaxation effects during the long mixing times involved in such experiments. Proton-assisted recoupling (PAR) methods relying on the third spin-assisted recoupling (TSAR) mechanism (Paëpe et al. 2008; Lewandowski et al. 2009a) have been employed to obtain faster ^{15}N - ^{15}N signal transfers leading to the establishment of longer $^{15}\text{N}_i$ - $^{15}\text{N}_{i\pm n}$ ($n \geq 2$) constraints (Lewandowski et al. 2009b), although some $^{15}\text{N}_i$ - $^{15}\text{N}_{i\pm 1}$ correlations available from the PDS scheme were not visible by PAR when carried out on the same sample system (Franks et al. 2006, 2005; Lewandowski et al. 2009b). This work explores the application of the recently proposed AL FRESKO scheme, to obtain this kind of ^{15}N - ^{15}N correlations in proteins under a variety of conditions. Advantages of the ensuing approach are illustrated, and potential extensions of this method briefly discussed.

Results

This work explored the application of direct ^{15}N - ^{15}N (Fig. 1a), and indirect ^1H - ^1H -driven (Fig. 2a) 2D AL FRESKO schemes (Fig. 1b), to obtain 2D ^{15}N - ^{15}N correlations under MAS. The AL FRESKO scheme (Wi and Frydman 2020) was originally applied to recouple ^{13}C - ^{13}C dipolar interactions, and proved particularly efficient under



fast MAS rates (~ 60 kHz). AL FRESCO involves storing the t_1 -encoded X-nuclei polarization along the z-axis ($X = {}^{13}\text{C}$ or ${}^{15}\text{N}$), and employing a phase-modulated chirped pulse—such as the wideband, uniform rate, smooth truncation (WURST)

(Kupce and Freeman 1995) or the hyperbolic secant (HS) (Baum et al. 1985; Silver et al. 1984) pulse—on the ${}^1\text{H}$ channel, in order to achieve the recoupling between the non-equivalent low- γ nuclei. This chirped mixing rf pulse

Fig. 2 a ^{15}N - ^{15}N 2D correlation sequence implemented using a ^1H - ^{15}N mixing scheme aided by either spontaneous spin diffusion (SD) or AL FRESKO pulses applied on the ^{15}N channel. Black lines indicate 90° pulses. Pulse phases: $\phi_1=(x)_2, (-x)_2, (y)_2, (-y)_2, (-x)_2, (x)_2, (-y)_2, (y)_2$; $\phi_2=(-y)_4, (x)_4, (y)_4, (-x)_4$; $\phi_3=(-x)_2, (x)_2, (-y)_2, (y)_2, (x)_2, (-x)_2, (y)_2, (-y)_2$; $\phi_4=y$; $\phi_5=y$; $\phi_6=-y, y$; $\phi_7=x$; $\phi_8=-x$; $\phi_9=y$; $\phi_{10}=(y)_2, (-y)_2, (-x)_2, (x)_2, (-y)_2, (y)_2, (x)_2, (-x)_2$; $\phi_{1x}=-y, y, -y, y, x, -x, x, -x, y, -y, y, -y, -x, x, -x, x$. **b-e** ^{15}N - ^{15}N correlation spectra of ^{15}N -labeled GB1 measured using ^1H - ^{15}N SD and ^1H - ^{15}N AL FRESKO sequences with mixing times of 1.2 ms (**b, d**) and 2 ms (**c, e**). While employing the MAS spinning rate $\nu_r=16$ kHz, the number of t_1 increments (n_{t_1}), total number of scans (ns), dwell time used in the indirect time domain (dw_{t_1}) and acquisition delay time (d_1) used in each experiment were $n_{t_1}=150$, $ns=160$, $dw_{t_1}=250$ μs and $d_1=2$ s, respectively. Comparing the SD (pink) and AL FRESKO (blue) derived strips collected for the 2 ms mixing case are shown separately in (**f**) and (**g**)

can be relatively weak, with an amplitude $\nu_{rf}=5\sim 20$ kHz regardless of the MAS rate employed—low-powers becoming a significant advantage when assessing long X-X distances, characterized by MAS-averaged couplings demanding extended mixing times. The chirped mixing pulses will then reintroduce the ^1H -X heteronuclear dipolar coupling despite the MAS averaging, by repeatedly satisfying the rotary resonance condition:

$$\nu_{\text{eff}}(^1\text{H}) = \left[\left\{ \Omega_H + \frac{\text{BW}}{2} - \left(\frac{\text{BW}}{t_p} \right) t \right\}^2 + \left\{ \nu_{rf}^{\text{env}}(t) \right\}^2 \right]^{1/2} = \nu_r, \quad (1)$$

where $\nu_{\text{eff}}(^1\text{H})$ is the effective ^1H rf strength, Ω_H is the ^1H frequency offset, BW is the chirp's sweep bandwidth, t_p is the chirp's pulse length, $\nu_{rf}^{\text{env}}(t)$ is the time-varying rf pulse strength considered with the envelope shape of the chirp, and ν_r is the sample MAS rate. The ^1H -X heteronuclear dipolar couplings thus introduced can then reestablish a homonuclear X_1 - X_2 coupling, by broadening the homonuclear transfer otherwise given by a narrow rotational resonance condition, $\Delta\Omega = \nu_{X_1} - \nu_{X_2} = \nu_r$. As described previously (Wi and Frydman 2020), AL FRESKO mixing effectiveness also benefits from the application of an under-sampled chirped scheme whereby $1/\Delta t \ll \text{BW}$, where Δt is the dwell time used to clock out the pulse. This deviates from the usual Nyquist sampling condition $1/\Delta t \geq \text{BW}$ required to avoid frequency folding, and implies that frequency points within the $1/\Delta t$ frequency window are addressed multiple times during the course of a single frequency sweep—in other words, that the X_1 - X_2 signal transfer conditions within a $1/\Delta t$ window are satisfied multiple times. This ends up enhancing the transfer efficiency for a given mixing time.

Figures 1c-e compare variable-rate 2D MAS ^{15}N - ^{15}N correlation spectra collected on uniformly ^{15}N , ^{13}C -labeled GB1, using a PDSM mixing scheme (first column) with $\tau_{\text{mix}}=6.25$ s, and the AL FRESKO mixing scheme (second

column) with a mixing time of 6.25 s and an average effective rf pulse strength of $\overline{\nu_{rf}^{\text{env}}}=5.3$ kHz. The MAS spinning rates used were 12 kHz (c), 16 kHz (1d), and 19 kHz (1e), respectively. In each case, four identical HS mixing pulses (1% truncation) were used in series, while shifting phases and changing the direction of the sweep as shown in the figure, with $t_p=1.5625$ s, $\Delta t=3/\nu_r$, $N=t_p/\Delta t$, and $\text{BW}=80$ kHz. Thus, the overall AL FRESKO mixing time was $4N\Delta t=6.25$ s in all cases. As the MAS rate increases the number of ^{15}N - ^{15}N cross-peaks in both PDSM and AL FRESKO spectra decrease; however, at each MAS rate, the AL FRESKO experiment clearly delivers ^{15}N - ^{15}N cross-peaks (red contours) that are missing in the conventional PDSM spectrum. This observation can be justified by the fact that AL FRESKO, as a derivative of the dipole-assisted rotational resonance (DARR) technique, will produce X_1 - X_2 cross-peaks more efficiently than a non-recoupled PDSM experiment. The Supporting Information presents simulations that further support this premise (see Supporting Fig. S1a, b). Notice as well that DARR would require its rf pulse power to increase with MAS rate in order to keep on matching a $\nu_{rf}=\nu_r$ condition, whereas AL FRESKO requires much weaker rf powers even as the MAS rate increases, owing to its reliance on effective fields. The data in Fig. 1 are complemented with PDSM and AL FRESKO GB1 spectra measured at shorter mixing times (2 s) at three different MAS rates, $\nu_r=12, 16$, and 19 kHz. As can be appreciated from Supporting Figure S2, these spectra exhibit significantly fewer cross peaks than these spectra measured with $\tau_{\text{mix}}=6.25$ s; yet also in that instance, AL FRESKO reveals connectivities that are lost in the PDSM data.

An alternative route that can significantly increase the number of ^{15}N - ^{15}N correlations while reducing the length required by the mixing time, is to employ a ^1H - ^{15}N mixing method. This calls for an $^{15}\text{N} \rightarrow \text{H} \rightarrow \text{H} \rightarrow ^{15}\text{N}$ pulse scheme of the kind shown in (Fig. 2a) (de Boer et al. 2002; Lange et al. 2003; Aluas et al. 2009; Kobayashi et al. 2017) where, after the first ^1H - ^{15}N CP step, ^{15}N magnetizations that evolved over a time t_1 are sent back to the ^1H reservoir via a 2^{nd} $^{15}\text{N} \rightarrow ^1\text{H}$ CP step for longitudinal ^1H - ^{15}N mixing. This can proceed either by spontaneous spin diffusion (SD), AM-MIRROR (Wittmann et al. 2016), or aided by AL FRESKO mixing pulses, applied this time on the ^{15}N species. Following this, ^1H magnetizations are transferred again to the ^{15}N channel for detection via a final $^1\text{H} \rightarrow ^{15}\text{N}$ CP step; chirped ^{15}N pulses would then be used in this AL FRESKO scheme to aid the ^1H - ^{15}N mixing.

Figures 2b-e show ^{15}N - ^{15}N correlation spectra of GB1 collected in this fashion, by relying on spontaneous ^1H - ^{15}N spin diffusion (2b, 2c) and on AL FRESKO (2c, 2e) mixing schemes. These MAS data were collected

at $\nu_r = 16$ kHz, using mixing times of $\tau_{\text{mix}} = 1.2$ ms (2b, 2d) and 2 ms (2c, 2e); further details of the experimental parameters are specified in the figure caption and in the Experimental. Standing out against the low- γ -based dipolar mixing experiments in Fig. 1, are the many additional ^{15}N - ^{15}N correlations visible in these indirect $^1\text{H}^{\text{N}}$ - $^1\text{H}^{\text{N}}$ mixing experiments—despite their very short mixing times. Furthermore, as can be seen by comparing the spectra measured by $^1\text{H}^{\text{N}}$ - $^1\text{H}^{\text{N}}$ SD (2b and 2c) and $^1\text{H}^{\text{N}}$ - $^1\text{H}^{\text{N}}$ AL FRESKO (2d and 2e), additional ^{15}N - ^{15}N correlations are once again visible for the latter for both 1.2 ms and 2 ms mixing times (e.g., compare the 1D projection spectrum taken at ~ 109 ppm and shown in each 2D spectrum). This is more clearly illustrated by the strips extracted at ≈ 108 and 111 ppm for the two experiments measured with 2 ms, which show additional ^{15}N - ^{15}N correlations from the AL FRESKO scheme (Fig. 2f, g). A more thorough cross-comparison among all these experiments is presented in Supporting Tables S2 and S3, which summarize the $^{15}\text{N}_i$ - $^{15}\text{N}_j$ cross-peak correlations obtained both by the direct ^{15}N - ^{15}N and indirect $^1\text{H}^{\text{N}}$ - $^1\text{H}^{\text{N}}$ correlation experiments presented in Figs. 1 and 2. The first of these Tables summarizes correlations between nearest neighboring amino acids in the peptide sequence, whereas the second focuses on distant correlations. Table 1 complements these data by summarizing the number of N_i - N_j correlations found by 2D ^{15}N - ^{15}N correlation experiments carried out so far on U- ^{15}N -GB1, including conventional PDS (Franks et al. 2006), PAR (Lewandowski et al. 2009b), and the ^{15}N - ^{15}N AL FRESKO and $^1\text{H}^{\text{N}}$ - $^1\text{H}^{\text{N}}$ SD and AL FRESKO schemes. The $^1\text{H}^{\text{N}}$ - $^1\text{H}^{\text{N}}$ AL FRESKO scheme appears to give more correlations than any other alternative—including those that have been reported in the U- ^{15}N -GB1 solid-state NMR literature so far (Franks et al. 2006; Lewandowski et al. 2009b).

For completion, Fig. 3a and b compare the N_i - N_j correlations obtained by the direct ^{15}N - ^{15}N AL FRESKO and by the indirect $^1\text{H}^{\text{N}}$ - $^1\text{H}^{\text{N}}$ AL FRESKO scheme, respectively. Additionally shown in Fig. 3c are partial overlays from the 108–112, 115–119 and 131–134 ppm regions (F_1 domain), clearly evidencing the additional N_i - N_j correlations visible upon using the $^1\text{H}^{\text{N}}$ - $^1\text{H}^{\text{N}}$ mixing.

Discussion

^{15}N -based AL FRESKO mixing experiments do not appear substantially better than PDS-based ones when targeting nearest neighbor connectivities, but exceed the latter performance when seeking longer distances. Indeed most ^{15}N - ^{15}N correlations observed in the PDS experiment (Franks et al. 2006), are of the N_i - $\text{N}_{i\pm 1}$ type: 10 are in GB1's α -helix, 6 in its β -sheet, 10 in the loop region, and 13 at the loop \leftrightarrow β -sheet and loop \leftrightarrow α -helix interfaces. In addition, a few N_i - $\text{N}_{i\pm 2}$ correlations are also observed: 7 in the α -helix, 1 in a loop, and 2 from the interface loop \leftrightarrow α -helix and loop \leftrightarrow β -sheet. Being less affected by dipolar truncation, PAR shows a better ability to detect longer N_i - $\text{N}_{i\pm n}$ ($n \geq 2$) correlations (Lewandowski et al. 2009b): data revealed one such loop \leftrightarrow loop correlation; and 3 β -sheet \leftrightarrow β -sheet ones—even if some N_i - $\text{N}_{i\pm 1}$ and N_i - $\text{N}_{i\pm 2}$ correlations visible in the PDS experiment, are remarkably missing from the PAR experiment (see Table 1 and Supporting Tables S2 and S3). The ^{15}N - ^{15}N AL FRESKO experiment shows an increase in the number of N_i - $\text{N}_{i\pm n}$ ($n \geq 2$) correlations over the former two experiments. The data show 3 such loop \leftrightarrow loop correlations, 4 β -sheet \leftrightarrow β -sheet correlations, 1 loop \leftrightarrow β -sheet correlation, and 1 α -helix \leftrightarrow loop (Table 1). The method also increases the number of N_i - $\text{N}_{i\pm 2}$

Table 1 Number of N_i - N_j ($j=i \pm n$) correlations found in GB1 by various mixing schemes

n	Experiment	α -helix	β -sheet	Loop	Loop \leftrightarrow β -sheet	α -helix \leftrightarrow loop	Loop \leftrightarrow loop	β -sheet \leftrightarrow β -sheet
1	^{15}N - ^{15}N PDS ^a	10	6	10	10	3		
	^{15}N - ^{15}N PAR ^b	12	1	8	5	2		
	^{15}N - ^{15}N AL FRESKO	10	8	9	6	3		
	$^1\text{H}^{\text{N}}$ - $^1\text{H}^{\text{N}}$ SD	13	3	5	7	3		
	$^1\text{H}^{\text{N}}$ - $^1\text{H}^{\text{N}}$ AL FRESKO	14	10	12	14	4		
≥ 2	^{15}N - ^{15}N PDS ^a	7		1	1	1		
	^{15}N - ^{15}N PAR ^b	3			1		1	3
	^{15}N - ^{15}N AL FRESKO	16	2	2	1	1	3	4
	$^1\text{H}^{\text{N}}$ - $^1\text{H}^{\text{N}}$ SD	27	1	2	3	4	6	4
	$^1\text{H}^{\text{N}}$ - $^1\text{H}^{\text{N}}$ AL FRESKO	30	3	5	8	5	10	22

^aReference Franks et al. (2006)

^bReference Lewandowski et al. (2009b)

${}^1\text{H}^{\text{N}}_{i\pm 2}$ distances in a β -sheet structure motif are 6.8–7.1 Å long. Still, if multiple β -sheet chains form parallel or antiparallel registries, inter-registry $\text{N}_i\text{--}\text{N}_{i\pm n}$ ($n \geq 2$) correlations between nearby β -sheet structures can still be detected by the ${}^1\text{H}^{\text{N}}\text{--}{}^1\text{H}^{\text{N}}$ AL FRESKO scheme, as can be seen from Table 1 and Supporting Table S3.

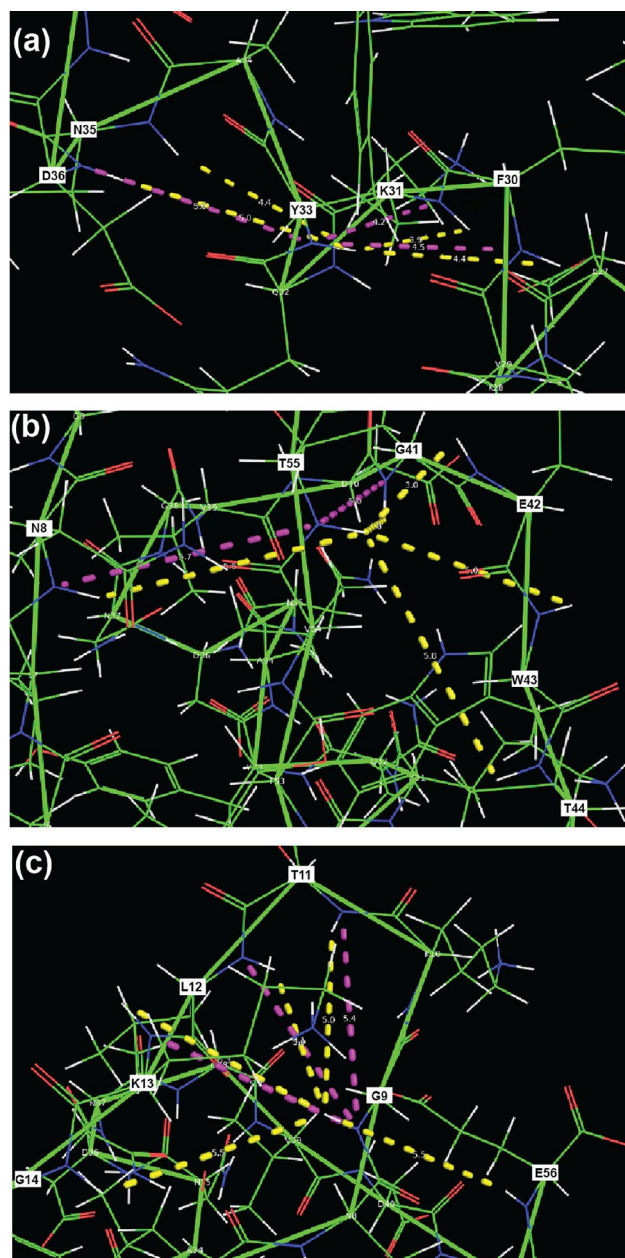


Fig. 4 Examples of structural constraints, $\text{N}_i\text{--}\text{N}_{i\pm n}$ and $\text{H}_i^{\text{N}}\text{--}\text{H}_{i\pm n}^{\text{N}}$ ($n > 2$), identified from the assigned correlations of the spectra shown in Fig. 3 in typical α -helix, antiparallel β -sheet registry, and β -turn motifs. Dashed pink lines represent correlations revealed by the $\text{N}_i\text{--}\text{N}_{i\pm n}$ mixing experiments, and dashed yellow lines represent correlations revealed by the $\text{H}_i^{\text{N}}\text{--}\text{H}_{i\pm n}^{\text{N}}$ tests. Further details about these correlations are summarized in Table 2

Figure 4 shows pictorial examples of long-range $\text{N}_i\text{--}\text{N}_{i\pm n}$ ($n \geq 2$) correlations found in α -helix (4a), β -sheet registry (4b), and β -loop (4c) motifs of GB₁, in the correlation data obtained by ${}^{15}\text{N}\text{--}{}^{15}\text{N}$ (6.5 s mixing time) and the ${}^1\text{H}^{\text{N}}\text{--}{}^1\text{H}^{\text{N}}$ (2 ms mixing time) AL FRESKO mixing schemes. Details of peak positions, distance constraints, and inter-residue distances n involved in these correlations are summarized in Table 2. In an α -helix structure (Fig. 4a), the Y33-K31, Y33-F30 and Y33-D36 correlations are visible in the ${}^{15}\text{N}\text{--}{}^{15}\text{N}$ AL FRESKO scheme (pink dashed lines); an additional Y33-N35 correlation is visible when using the indirect ${}^1\text{H}^{\text{N}}\text{--}{}^1\text{H}^{\text{N}}$ AL FRESKO mixing scheme (yellow dashed line). Figure 4b illustrates correlations formed between β -sheets and β -sheet structures in an antiparallel β -sheet registry for T55: the T55-G41 and T55-N8 correlations are visible from the direct ${}^{15}\text{N}\text{--}{}^{15}\text{N}$ AL FRESKO scheme, while additional T55-E42, T55-W43, and T55-T44 correlations appear when utilizing the indirect ${}^1\text{H}^{\text{N}}\text{--}{}^1\text{H}^{\text{N}}$ AL FRESKO scheme. Finally, Fig. 4c illustrates the $\text{N}_i\text{--}\text{N}_{i\pm n}$ ($n \geq 2$) correlations for residue G9 with nearby residues in a β -loop motif. There, G9-T11, G9-L12, and G9-K13 correlations are visible with the direct ${}^{15}\text{N}\text{--}{}^{15}\text{N}$ AL FRESKO scheme, while G9-T11, G9-L12, G9-K13, G9-G14 and G9-E56 correlations also arise with the indirect ${}^1\text{H}^{\text{N}}\text{--}{}^1\text{H}^{\text{N}}$ AL FRESKO scheme. Other long-range $\text{N}_i\text{--}\text{N}_{i\pm n}$ ($n \geq 2$) correlations formed for each GB₁ residue as examined by various mixing schemes, are summarized in the Table S3 of the Supporting Information.

Conclusion

This study examined the AL FRESKO mixing scheme as applied on uniformly ${}^{15}\text{N}$, ${}^{13}\text{C}$ -labeled GB₁ to obtain ${}^{15}\text{N}\text{--}{}^{15}\text{N}$ correlations under a moderately spinning rates via direct ${}^{15}\text{N}\text{--}{}^{15}\text{N}$ and indirect ${}^1\text{H}^{\text{N}}\text{--}{}^1\text{H}^{\text{N}}$ mixing schemes. A significant number of correlations, particularly long-range $\text{N}_i\text{--}\text{N}_{i\pm n}$ ($n \geq 2$), were produced with both cases. The usefulness of ${}^{15}\text{N}\text{--}{}^{15}\text{N}$ correlations relying on AL FRESKO schemes, particularly via ${}^1\text{H}^{\text{N}}\text{--}{}^1\text{H}^{\text{N}}$ mixing, is therefore proven for examining the protein secondary structures and three-dimensional arrangements in the solid-state NMR of polycrystalline systems. Overall, the constraints arising from the ${}^1\text{H}^{\text{N}}\text{--}{}^1\text{H}^{\text{N}}$ AL FRESKO scheme should help determine the three-dimensional arrangement of secondary structures in protein structures. We are currently extending the ${}^1\text{H}^{\text{N}}\text{--}{}^1\text{H}^{\text{N}}$ AL FRESKO scheme further to the case of ${}^1\text{H}$ -detection mode under a very fast MAS rate, as well as to experiments that—by introducing an additional ${}^{13}\text{C}$ -based dimension, can perform similar kind of correlations with the spectral enhancement afforded by 3D NMR.

Table 2 Representative N_i-N_j ($n = j - i \geq 2$) correlations found in ^{15}N - ^{15}N AL FRESKO and $^1\text{H}^{\text{N}}-^1\text{H}^{\text{N}}$ AI FRESKO mixing schemes

Pair	N_i ppm	N_j ppm	n	N_i-N_j Distance (Å)	$^{15}\text{N}-^{15}\text{N}$ 6.25 s	$\text{H}_i^{\text{N}} - \text{H}_j^{\text{N}}$ distance (Å)	$^1\text{H}^{\text{N}}-^1\text{H}^{\text{N}}$ 2 ms
T55-N8	124.6	124.9	47	5.7	✓	5.9	✓
T55-G41	124.6	109.2	14	4.9		4.5	✓
T55-E42	124.6	120.0	13	3.9	✓	3.1	✓
T55-W43	124.6	126.4	12	5.1		5.0	✓
T55-T44	124.6	109.4	11	6.7		5.7	✓
Y33-D36	121.5	121.2	3	5.0	✓	5.0	✓
Y33-N35	121.5	118.7	2	4.4		4.4	✓
Y33-F30	121.5	119.2	3	4.5	✓	4.4	✓
Y33-K31	121.5	121.9	2	4.2	✓	3.8	✓
G9-E56	109.8	132.0	47	5.5		5.4	✓
G9-G14	109.9	106.8	5	6.9		5.7	✓
G9-K13	109.8	123.7	4	5.3	✓	5.5	✓
G9-L12	109.8	127.8	3	5.0	✓	3.7	✓
G9-T11	109.8	109.7	2	5.4	✓	5.1	✓

Mutual correlations N_i-N_j and N_j-N_i are counted once as N_i-N_j

Experimental details

Sample

[U- ^{13}C , ^{15}N] GB1 was expressed in *E. coli* BL21-(DE3) cells that grew in minimal media (1 g/L $^{15}\text{NH}_4\text{Cl}$, 2 g/L ^{13}C glucose). This double-labeling was chosen over the simpler ^{15}N -only labeling for facilitating the peaks' assignments. Protein expression was induced with 1 mM isopropyl- β -D-thiogalactoside for 4 h. The protein was purified by anion exchange using a Q-Sepharose FF column, followed by gel filtration on a Superdex-75 column. Peak fractions were pooled and concentrated with Centrplus 3 kDa MWCO filters, and the buffer solution was thoroughly exchanged to 20 mM sodium phosphate at pH 8.0. To obtain highly resolved ^{15}N NMR spectra a microcrystalline GB1 powder was prepared by following the precipitation procedure of Franks et al. (2005) In this, about 3.6 mL aliquots of a mixture of isopropanol (1.2 mL) and 2-methylpentane-2,4-diol (2.4 mL) were added dropwise to 1.2 mL of a 30 mg/mL solution of GB1 in phosphate buffer (pH 5.5), while mixing the solution thoroughly using a vortex. The resultant solution was left at room temperature for about 30 min and then, the milky protein precipitate was centrifugated. The pellet was packed into 3.2 mm pencil type NMR rotors by centrifugation using a home-made swing bucket for rotor packing.

NMR experiments

NMR experiments were carried out on an 18.8 T magnet equipped with a Bruker Avance III HD console using a

3.2 mm ^1H -X-Y low-E NHMFL-built MAS probe. MAS spinning rates of 12, 16 and 19 kHz were used for the direct ^{15}N - ^{15}N correlations scheme, and 16 kHz for the indirect scheme relying on the $^1\text{H}^{\text{N}}-^1\text{H}^{\text{N}}$ mixing. The sample temperature was regulated at -10 °C (measured at the sample compartment) by flowing a nitrogen gas stream generated from a liquid nitrogen tank via an FTS cooling system. ^1H , ^{13}C and ^{15}N 90° pulses were adjusted to 2.5 μs , 5 μs , and 9 μs , respectively, for all the experiments. For the direct ^{15}N - ^{15}N mixing scheme, an optimal ^1H - ^{15}N cross-polarization (CP) condition at each spinning rate was found at $\nu_1(^{15}\text{N}) = 27$ kHz and $\nu_1(^1\text{H}) = 50 \sim 70$ kHz depending on the MAS rate; a rectangular pulse along the ^{15}N channel and a simultaneous ramped (70%–110%) spin-lock pulse along ^1H channel for 700 μs , were used for CP. For the indirect $^1\text{H}^{\text{N}}-^1\text{H}^{\text{N}}$ mixing scheme (Boer et al. 2002; Lange et al. 2003), 700 μs long rectangular spin-lock pulses with an identical ^{15}N pulse power, $\nu_1(^{15}\text{N}) = 27$ kHz, were used along the ^{15}N channel at the 1st ^1H - ^{15}N CP; the 2nd ^{15}N - ^1H CP lasted 240 μs , and the 3rd ^1H - ^{15}N CP for 420 μs . A ramped (70%–110%) spin-lock pulse was applied simultaneously along the ^1H channel in each case with rf powers of $\nu_1(^1\text{H}) = 54$ kHz, 47 kHz, and 53 kHz, respectively. SPINAL-64 (Fung et al. 2000) (90 kHz rf field) was applied for ^1H decoupling during the direct and indirect evolution/acquisition periods; no ^{13}C decoupling was used, as tests did not reveal any ^{15}N line shape improvements deriving from it. Two-dimensional (2D) NCO/NCA MAS experiments ($\nu_r = 16$ kHz) (Baldus et al. 1998; Polenova and Ramamoorthy 2006) were carried out for peak assignment purposes. The rf pulse parameters used were: first ^1H - ^{15}N CP with $\nu_1(^{15}\text{N}) = 27$ kHz and $\nu_1(^1\text{H}) = 68$ kHz for 700 μs while

applying a ramped spin-lock (70–110%); second ^{15}N – ^{13}C CP with $\nu_1(^{15}\text{N})=30$ kHz and $\nu_1(^{13}\text{C})=45$ kHz for 5 ms with a ramped spin-lock pulse (70–110%) applied along ^{13}C while placing the ^{13}C 's offset carrier frequency at CO peaks and $\text{C}\alpha$ peaks for NCO and NCA, respectively. 128 t_1 slices were taken with a dwell time of 250 μs for both NCO and NCA. Each t_1 point was produced by coadding 128 scans with an acquisition delay time of 2 s.

Chirp mixing pulse design

Wideband, uniform rate, smooth truncation (WURST) and hyperbolic secant (HS) chirped pulses (Kupce and Freeman 1995; Garwood and Barre 2001), were used for the AL FRESKO experiments. While it was possible to obtain similar spectra using either one of these waveforms, it was generally seen that when directly mediated by ^{15}N – ^{15}N interactions, HS- m pulses with $m \leq 5$ (m being the truncation level) performed slightly better, while when proceeding via ^1H – ^1H mixing WURST- n pulses (with $n \geq 40$ being the power of the cosine envelope function) were better. Hence HS pulses were used in collecting the data shown in Fig. 1, while WURST ones were used to collect the data in Fig. 2. Both of these pulses were constructed using the Topspin's shaped pulse waveforming menu, with a dwell time (Δt) = $3/\nu_r$, sweep bandwidth (BW) = 40–80 kHz, and number of digital points (N) = $t_p/\Delta t$, where ν_r is the MAS spinning rate and t_p is the chirp pulse duration. Normally $t_p = \tau_{\text{mix}}$, where τ_{mix} is the mixing time; however, for long mixing times such as $\tau_{\text{mix}} = 5$ s or 6.25 s, τ_{mix} was divided into n chirp pulses with an identical t_p and having a phase alternation scheme $\text{X}\bar{\text{X}}\text{Y}\bar{\text{Y}}\dots$, where X or Y is the initial phase of an individual chirp pulse and ζ ($\zeta = \text{X}$ or Y) and $\bar{\zeta}$ are a forwardly and backwardly swept chirped pulses, respectively. An HS pulse scheme with a 1–5% of truncation level and a WURST pulse scheme with the smallest even amplitude power $n=2$ were optimal for maximizing ^{15}N – ^{15}N correlations when using these long mixing time. Since these WURST or HS schemes employed a weak rf pulse power (maximum amplitude ~5–20 kHz) regardless of the MAS rate, the effective rf pulse power ($\overline{v_{rf}^{env}}$) of the resultant chirped pulses was significantly low and allowed the total mixing period to be extended up to a few seconds without inducing any serious rf heating effect on the sample. For instance, the rf pulse strength of the HS pulse scheme used in Fig. 1b was at its maximum amplitude 11 kHz; considering the amplitude shape of the HS pulse with a truncation level of 1%, the effective rf pulse strength ($\overline{v_{rf}^{env}}$) employed for the overall mixing time was only 0.48×11 kHz = 5.3 kHz. More details in designing a suitable chirp pulse scheme for the AL FRESKO mixing scheme were described in a previous publication (Wi and Frydman 2020). For the short chirp pulse

scheme applied along the ^{15}N channel in the indirect ^1H – ^1H mixing scheme, we employed $\Delta t = 1/\nu_r$, BW = 40–80 kHz, and $N = t_p/\Delta t$ with $\tau_{\text{mix}} = t_p$ (≤ 2 ms). In this case a WURST type with $n=80$ was found optimal with $\nu_1(^{15}\text{N})=25$ kHz based on our numerical simulations carried out on a model 6-spin cluster, $^{15}\text{N}_1^1\text{H}_1$ – $^{15}\text{N}_2^1\text{H}_2$ – $^{15}\text{N}_3^1\text{H}_3$, shown in the Supporting Fig. S1.

Chemical shift assignments of GB1

To obtain backbone chemical shift assignments (N, $\text{C}\alpha$, C') for GB1, NCA and NCO experiments were used. Spectra were acquired and processed by TopSpin, and the processed frequency domain spectra were analyzed using the POKY suite (BUILD 082522) after conversion to the UCSF format (Lee et al. 2021). The *BMRB entry download* button in the *Resonances* tab of POKY was used to import chemical shifts published by the Rienstra group (BMRB entry number 15380) (Frericks-Schmidt et al. 2007). Then, we generated peaks with an assignment label by the *Transfer and Simulate* tool (two-letter-code *TA*) on NCA and NCO. During this peak propagation step, we performed re-referencing of the spectra (two-letter-code *st*), by comparing uniform chemical shift differences between signals on our spectra and the simulated peak positions. After that, peak positions were fine-tuned by careful visual inspection. Figure S3 in the Supporting material illustrates assignments on representative NCA and NCO spectra.

Assignments of the ^{15}N – ^{15}N and $^{15}\text{N}(^1\text{H}^1\text{H})^{15}\text{N}$ spectra

To identify long-range signals on the ^{15}N – ^{15}N and $^{15}\text{N}^1\text{H}^1\text{H}^{15}\text{N}$ spectra, GB1 coordinates were downloaded from the Protein Data Bank (PDB ID 2GI9) and hydrogen atoms attached using a POKY Notepad script *attach_hydrogen_to_pdb.py* available in the POKY github repository (<https://github.com/pokynmr>). Then, the POKY Notepad script *ssnmr_NNpeak_maker_using_pdb.py*, which calculates interatomic distances and places peaks with an assignment label if two atoms are closer than the cutoff distance specified by the user, was applied, specifying 5 Å as a cutoff for the distance between two amide hydrogen atoms. Many of ^{15}N signals overlapped on 2D spectra. The POKY script was particularly useful because we did not have to pick peaks manually. Generated peaks were sorted by data heights in the peak list window of POKY, and only peaks falling on a signal were accepted.

Supplementary Information The online version contains supplementary material available at <https://doi.org/10.1007/s10858-023-00429-0>.

Acknowledgements This work was performed at the National High Magnetic Field Laboratory, which is supported by National Science Foundation Cooperative Agreement No. DMR-2128556 and the State of Florida. WL acknowledges a partial support from the National Science Foundation (Grant No. DBI-2051595). Supports from the Israel Science Foundation (Grant No. 1874/22) and the Perlman Family Foundation are gratefully acknowledged by LF. LF holds the Bertha and Isadore Gudelsky Professorial Chair and heads the Clore Institute for High-Field Magnetic Resonance Imaging and Spectroscopy (Weizmann Institute) whose support is also acknowledged.

Author contributions SW performed NMR experiments, data analysis, and drafted manuscript. KP and WL carried out peak assignments of two-dimensional NMR spectra. CL provided ^{15}N , ^{13}C -labeled GB1 sample. LF provided idea discussion and final manuscript review. All authors reviewed the manuscript.

Declarations

Competing interests The authors declare no competing interests.

References

- Aluas M, Tripon C, Griffin JM, Filip X, Ladizhansky V, Griffin RG, Brown SP, Filip C (2009) CHHC and 1H–1H magnetization exchange: analysis by experimental solid-state NMR and 11-spin density-matrix simulations. *J Magn Reson* 199:173–187
- Baldus M, Petkova AT, Herzfeld J, Griffin RG (1998) Cross polarization in the tilted frame: assignment and spectral simplification in heteronuclear spin systems. *Mol Phys* 95:1197–1207
- Baum J, Tycko R, Pines A (1985) Broadband and adiabatic inversion of a two-level system by phase-modulated pulses. *Phys Rev A* 32:3435–3447
- Bayro MJ, Huber M, Ramachandran R, Davenport TC, Meier BH, Ernst M, Griffin RG (2009) Dipolar truncation in magic-angle spinning NMR recoupling experiments. *J Chem Phys* 130:114506
- Bennett AE, Ok JH, Griffin RG, Vega S (1992) Chemical shift correlation spectroscopy in rotating solids: radio frequency-driven dipolar recoupling and longitudinal exchange. *J Chem Phys* 96:8624–8627
- Brinkmann A, Levitt MH (2001) Symmetry principles in the nuclear magnetic resonance of spinning solids: heteronuclear recoupling by generated Hartmann-Hahn sequences. *J Chem Phys* 115:357–384
- de Boer I, Bosman L, Raap J, Oschkinat H, de Groot HJM (2002) 2D ^{13}C - ^{13}C MAS NMR correlation spectroscopy with mixing by true 1H spin diffusion reveals long-range intermolecular distance restraints in ultra-high magnetic field. *J Magn Reson* 157:286–291
- De Paëpe G, Lewandowski JR, Loquet A, Böckman A, Griffin RG (2008) Proton assisted recoupling and protein structure determination. *J Chem Phys* 129:245101
- Donovan KJ, Silvers R, Linse S, Griffin RG (2017) 3D MAS NMR experiment utilizing through-space ^{15}N – ^{15}N correlations. *J Am Chem Soc* 139:6518–6521
- Franks WT, Zhou DH, Wylie BJ, Money BG, Graesser DT, Frericks HL, Sahota G, Rienstra CM (2005) Magic-angle spinning solid-state NMR spectroscopy of the beta1 immunoglobulin binding domain of protein G (GB1): ^{15}N and ^{13}C chemical shift assignments and conformational analysis. *J Am Chem Soc* 127:12291–12305
- Franks WT, Wylie BJ, Stellfox SA, Rienstra CM (2006) Backbone conformational constraints in a microcrystalline U- ^{15}N -labeled protein by 3D dipolar-shift solid-state NMR spectroscopy. *J Am Chem Soc* 128:3154–3155
- Frericks-Schmidt HL, Sperling LJ, Gao YG, Wylie BJ, Boettcher JM, Wilson SR, Rienstra CM (2007) Crystal polymorphism of protein GB1 examined by solid state NMR spectroscopy and X-ray diffraction. *J Phys Chem B* 111:14362–14369
- Fung BM, Khitritin AK, Ermolaev K (2000) An improved broadband decoupling sequence for liquid crystals and solids. *J Magn Reson* 142:97–101
- Garwood M, de la Barre L (2001) The return of the frequency sweep: designing adiabatic pulses for contemporary NMR. *J Magn Reson* 153:155–177
- Giraud N, Blackledge M, Bockmann A, Emsey L (2007) The influence of nitrogen-15 proton-driven spin diffusion on the measurement of nitrogen-15 longitudinal relaxation times. *J Magn Reson* 184:51–61
- Goldbourn A, Day LA, McDermott AE (2007) Assignment of congested NMR spectra: Carbonyl backbone enrichment via the Entner-Doudoroff pathway. *J Magn Reson* 189:157–165
- Grommek A, Meier BH, Ernst M (2006) Distance information from proton-driven spin diffusion under MAS. *Chem Phys Lett* 427:404–409
- Hou G, Sun S, Han Y, Byeon I-J, Ahn J, Concel J, Samoson A, Gronenborn AM, Polenova T (2011) Spin diffusion driven by R-symmetry sequences: applications to homonuclear correlation spectroscopy in MAS NMR of biological and organic solids. *J Am Chem Soc* 133:3943–3953
- Hou G, Yan S, Trébosc J, Amoureux J-P, Polenova T (2013) Broadband homonuclear correlation spectroscopy driven by combined $\text{R}2(\text{n})(\text{v})$ sequences under fast magic angle spinning for NMR structural analysis of organic and biological solids. *J Magn Reson* 232:18–30
- Hu B, Lafon O, Trébosc J, Chen Q, Amoureux J-P (2011) Broadband homonuclear correlations assisted by 1H irradiation for biomolecules in very high magnetic field at fast and ultra-fast MAS frequencies. *J Magn Reson* 212:320–329
- Hu B, Trébosc J, Lafon O, Chen Q, Masuda Y, Takegoshi K, Amoureux J-P (2012) Very-long-distance correlations in proteins revealed by solid-state NMR spectroscopy. *ChemPhysChem* 13:3585–3588
- Kühne SR, Mehta MA, Stringer JA, Gregory DM, Shiels JC, Drobny GP (1998) Distance measurements by dipolar recoupling two-dimensional solid-state NMR. *J Phys Chem A* 102:2274–2282
- Kobayashi T, Slowing II, Pruski M (2017) Measuring long-range ^{13}C – ^{13}C correlations on a surface under natural abundance using dynamic nuclear polarization-enhanced solid-state nuclear magnetic resonance. *J Phys Chem C* 121:24687–24691
- Kupce E, Freeman R (1995) Adiabatic pulses for wideband inversion and broadband decoupling. *J Magn Reson A* 115:273–276
- Lange A, Seidel K, Verdier L, Luca S, Baldus M (2003) Analysis of proton-proton transfer dynamics in rotating solids and their use for 3D structure determination. *J Am Chem Soc* 125:12640–12648
- Lee YK, Kurur ND, Helmle M, Johannessen OG, Nielsen NC, Levitt MH (1995) Efficient dipolar recoupling in the NMR of rotating solids. A sevenfold symmetric radiofrequency pulse sequence. *Chem Phys Lett* 242:304–309
- Lee W, Rahimi M, Lee Y, Chiu A (2021) POKY: a software suite for multidimensional NMR and 3D structure calculation of biomolecules. *Bioinformatics* 37:3041–3042
- Levitt MH (2002) Symmetry-based pulse sequences in magic-angle spinning solid-state NMR. *Encycl Nucl Magn Reson* 9:165–196
- Lewandowski JR, De Paëpe G, Eddy MT, Struppe J, Maas JW, Griffin RG (2009a) Proton assisted recoupling at high spinning frequencies. *J Phys Chem B* 113:9062–9069
- Lewandowski JR, De Paëpe G, Eddy MT, Griffin RG (2009b) ^{15}N – ^{15}N proton assisted recoupling in magic angle spinning NMR. *J Am Chem Soc* 131:5769–5776

- Marulanda D, Tasayco ML, McDermott A, Cataldi M, Arriaran V, Polenova T (2004) Magic angle spinning solid-state NMR spectroscopy for structural studies of protein interfaces. Resonance assignments of differentially enriched *Escherichia coli* thioredoxin reassembled by fragment complementation. *J Am Chem Soc* 126:16608–16620
- Meier BH (1994) Polarization transfer and spin diffusion in solid state NMR. Academic Press, New York
- Morcombe CR, Gaponenko V, Byrd RA, Zilm KW (2004) Diluting abundant spins by isotope edited radio-frequency field assisted diffusion. *J Am Chem Soc* 126:7196–7197
- Nielsen NC, Blidsøe H, Jakobsen HJ, Levitt MH (1994) Double-quantum homonuclear rotary resonance: efficient dipolar recovery in magic-angle spinning nuclear magnetic resonance. *J Chem Phys* 101:1805–1812
- Polenova T (2006) Resonance assignments and secondary structure determination in uniformly and differentially enriched proteins and protein reassemblies by magic-angle spinning nuclear magnetic resonance spectroscopy. In: Ramamoorthy A (ed) NMR spectroscopy of biological solids. CRC Taylor & Francis, Boca Raton, p 57
- Raleigh DP, Levitt MH, Griffin R (1988) Rotational resonance in solid state NMR. *Chem Phys Lett* 146:71–76
- Reif B, Hohwy M, Jaroniec CP, Rienstra CM, Griffin RG (2000) NH-NH vector correlation in peptides by solid-state NMR. *J Magn Reson* 145:132–141
- Scholz I, Huber M, Manolikas T, Meier BH, Ernst M (2008) MIRROR recoupling and its application to spin diffusion under fast magic-angle spinning. *Chem Phys Lett* 460:278–283
- Shen M, Liu Q, Trébosc J, Lafon O, Masuda Y, Takegoshi K, Amoureux J-P, Hu B, Chen Q (2013) Exploring various modulation-sideband recoupling conditions of SHA+ sequence at fast MAS. *Solid State Nucl Magn Reson* 55–56:42–47
- Siedel K, Etzkorn M, Heise H, Becker S, Baldus M (2005) High-resolution solid-state NMR studies on uniformly [¹³C,¹⁵N]-labeled ubiquitin. *ChemBioChem* 6:1638–1647
- Silver MS, Joseph RI, Hoult DI (1984) Highly selective $\pi/2$ and π pulse generation. *J Magn Reson* 59:347–351
- Sun BQ, Costa PR, Kocisko D, Lansburt PT, Griffin RG (1995) Internuclear distance measurements in solid state nuclear magnetic resonance: dipolar recoupling via rotor synchronized spin locking. *J Chem Phys* 102:702–707
- Szeverenyi NM, Sullivan MJ, Maciel GE (1982) Observation of spin exchange by two-dimensional Fourier transform ¹³C cross-polarization magic-angle spinning. *J Magn Reson* 47:462–475
- Takegoshi K, Nakamura S, Terao T (2001) ¹³C–¹H dipolar-assisted rotational resonance in magic-angle spinning NMR. *Chem Phys Lett* 344:631–637
- Takegoshi K, Nakamura S, Terao T (2003) ¹³C–¹H dipolar-driven ¹³C–¹³C recoupling without ¹³C irradiation in nuclear magnetic resonance of rotating solids. *J Chem Phys* 118:2325–2341
- Tycko R (2008) Theory of stochastic dipolar recoupling in solid-state nuclear magnetic resonance. *J Phys Chem B* 112:6114–6121
- Tycko R, Dabbagh G (1990) Measurement of nuclear magnetic dipole–dipole couplings in magic angle spinning NMR. *Chem Phys Lett* 173:461–465
- van Rossum B-J, Castellani F, Pauli J, Rehbein K, Hollander J, de Groot HJM, Oschkinat H (2003) Assignment of amide proton signals by combined evaluation of HN, NN and HNCA MAS-NMR correlation spectra. *J Biomol NMR* 25:217–223
- Verel R, Baldus M, Ernst M, Meier BH (1998) A homonuclear spin-pair filter for solid-state NMR based on adiabatic-passage techniques. *Chem Phys Lett* 287:421–428
- Weingarth M, Demco DE, Bodenhausen G, Tekely P (2009) Improved magnetization transfer in solid-state NMR with fast magic-angle spinning. *Chem Phys Lett* 469:342–348
- Weingarth M, Bodenhausen G, Tekely P (2010) Broadband magnetization transfer using moderate radio-frequency fields for NMR with very high static fields and spinning speeds. *Chem Phys Lett* 488:10–16
- Wi S, Frydman L (2020) An efficient, robust new scheme for establishing broadband homonuclear correlations in biomolecular solid state NMR. *Chem Phys Chem* 21:284–294
- Wittmann JJ, Agarwal V, Hellwagner J, Lends A, Cadalbert R, Meier BH, Ernst M (2016) Accelerating proton spin diffusion in perdeuterated proteins at 100 kHz MAS. *J Biomol NMR* 66:233–242
- Yan XJ, Hu B (2016) Probing ¹⁵N–¹⁵N correlations in g-C₃N₄ samples with solid-state NMR SHA+ pulse sequence. *Chinese J Magn Reson* 33:361–367

Publisher's Note Springer Nature remains neutral with regard to jurisdictional claims in published maps and institutional affiliations.

Springer Nature or its licensor (e.g. a society or other partner) holds exclusive rights to this article under a publishing agreement with the author(s) or other rightsholder(s); author self-archiving of the accepted manuscript version of this article is solely governed by the terms of such publishing agreement and applicable law.